03-02-2014

Manuscript for

Proofs to: Dr Vanessa Tabernero

Departamento de Química Orgánica y Química Inorgánica

Universidad de Alcalá

Edificio de Farmacia, Campus Universitario

28871-Alcalá de Henares, Spain.

Enhanced activity of clays and its crucial role for the activity in olefin polymerization

Claudimar Camejo-Abreu[1], Vanessa Tabernero[1,*], María Dolores Alba[2], Tomás Cuenca[1,*], Pilar Terreros[3].

1 Departamento de Química Orgánica y Química Inorgánica, Universidad de Alcalá, Campus Universitario, E–28871 Alcalá de Henares, Spain.

2 Instituto de Ciencia de Materiales de Sevilla, Universidad de Sevilla-CSIC, 41092, Sevilla, Spain.

3 Instituto de Catálisis y Petroleoquímica, CSIC, Cantoblanco, 28049 Madrid, Spain

(*) Corresponding author: Tel.: +34-918854629
Fax.: +34-918854683

Email:vanessa.tabernero@uah.es

ABSTRACT

This paper presents a study of the effects of different treatments on the polymerization activity of modified clays as cocatalysts. To achieve this goal, an intercalating cation was introduced into two smectites and these clays were then modified with trimethyl aluminium. Upon examination of the results following ethylene polymerization, when a zirconocene complex was used as catalyst, and after an exhaustive structure analysis, interesting deductions about the generation mode of the active species were obtained. All active materials employed as support activators simultaneously presented aluminium in a pentahedral environment together with acidic hydrogen atoms. These two features were detected only after TMA treatment and they seem to be crucial elements in active cocatalyst generation. Moreover, a material without structural aluminium displayed the best activity pointing to the new aluminium species generated in the solid matrix as the determining factor for the activity. We proposed a synergic effect between Lewis acid aluminium centres and acidic Brönsted protons that generate the SiOHAl groups that activate the zirconium compound.

1. Introduction

α-Olefin polymerization catalyst systems that combine a Group IV metallocene complex and methylaluminoxane (MAO) as cocatalyst [1] were largely studied because these systems produce polyolefins with defined microstructures by selecting the appropriate structure of the metallocene complex [2-4]. Although the complex role of MAO in the polymerization reaction has not been fully elucidated yet; it is well known [5-8] that the active species must be obtained by an activator (cocatalyst) with acidic properties. On the basis of these findings, a large number of materials with Lewis or Brönsted-acidic sites have been tested as activators for the development of a MAO free catalyst system [9-11]. Recently, we have reported [12] the use of commercial materials (K10 and K30) chemically modified with AlR_3 (R = Me, TMA; R = Et, TEA) as supports and activators, dubbed "support activators". In the presence of group 4 metal precatalyst compounds, these catalytic systems were active for ethylene polymerization. However, it was not possible to establish a correlation between activity and structural features due to the high level of impurities in the K10 and K30 materials. Therefore, the aim of this research work was to select a set of pure clay minerals as starting materials in order to establish this good correlation.

The selected clay minerals were smectite-types and belonged to the family of 2:1 phyllosilicates [13]. Their crystalline structure is composed of stacked layers made of two silica tetrahedrons fused to an edge-shared octahedral sheet of aluminium or magnesium hydroxide. The isomorphic substitutions origin negative charges in the layers and their electroneutrality results from the cations residing in the interlayer space.

In order to understand the properties of clays that govern their catalytic properties[14, 15], the study of two smectites (montmorillonite and hectorite), both octahedrally charged, with different compositions has been included. The most straightforward way to change the acid strength and concentration of the acid centres is to substitute the interlayer cations (smectite/M^{n+}). Moreover we treated these materials with TMA and consequently we generated different support activators (smectite/M^{n+}/TMA).

In this study, we show the effect of the intrinsic nature of the material, the effect of the exchanged cations intercalated into the clay mineral layers before polymerization, and the result of TMA treatment on the acidic properties and catalytic performance on ethylene polymerization of different clays. The support activators obtained were fully characterized by several techniques including, XRD, XRF, FTIR and MAS-NMR. Their physical properties were correlated with the catalytic activity of the systems generated. The choice of these types of materials as support activators is warranted because of their laminar structure. The active species can be stabilized in the interlaminar space because of its cationic nature and the swelling capacity of these materials allows the polymer chain to grow.

Because acidity[16-18] is fundamental to the behaviour of these clay minerals as cocatalysts, it is interesting to note the expected surface acidity may be explained in terms of structure. Clay mineral Lewis acidity generally arises from exposed Al^{3+}, Mg^{2+} or other ions at the edges and dominates when the interlayer water is largely removed. Brönsted acidity arises from silanol structural groups or from protons formed by the dissociation of interlayer water caused by the polarizing effect of aluminium cations present in this space. In the cases of acid treatment it also arises from the exchange with H^+ ions.

With this in mind, the different treatments were chosen to influence the inherent acidity of these materials with the assumption that the mechanism for the generation of the active specie responsible for the polymerization would be similar to that proposed in homogeneous systems (Fig. 1) [19].

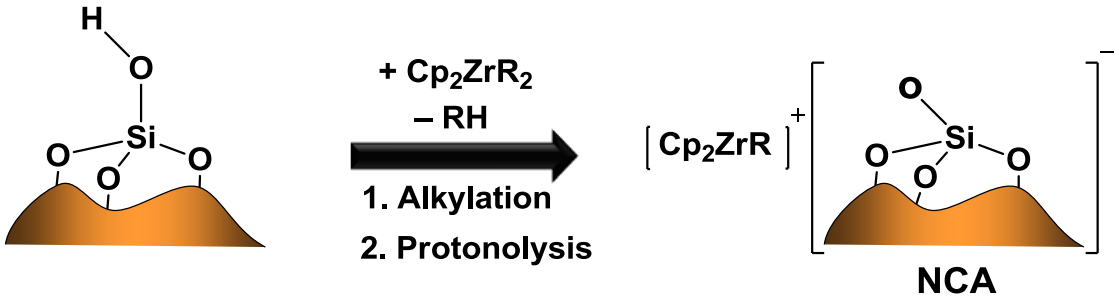

a. Activation via Brönsted acidity.

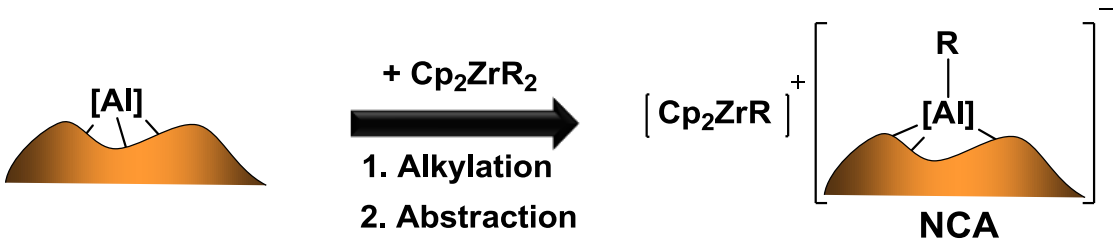

b. Activation via Lewis acidity.

Fig. 1. Possible pathways to active species generation.

2. Experimental

2.1. Starting materials and general conditions.

The smectite samples montmorillonite SAz-2 (MMt) and hectorite SHCa-1 (Hect) were supplied by the Source Clays Repository of Clay Minerals Society. Fractions smaller

than 2 μm were extracted [20], and the inorganic and organic matter [21, 22] were eliminated to give the starting materials, a montmorillonite termed MMt (cationic exchange capacity CEC = 156 meq/100g) and a hectorite termed Hect (CEC = 245 meq/100 g) respectively.[23] The samples were tested in different steps; with their natural interlaminar cations, when they were homoionized to obtain the cation-exchanged derivatives, and finally after TMA treatment.

$[Zr(\eta^5\text{-}C_5H_5)\{\eta^5\text{-}C_9H_6SiMe_2(CH_2CH{=}CH_2)\}Cl_2]$ was synthesized according to literature procedures.[24] All manipulations involving air sensitive compounds and materials were performed under Argon (Air Liquid, with O_2 and H_2O content below 3 ppm), using standard Schlenk and vacuum line techniques or in a MBraun Model 150-BG glove box continuously purged with high purity dry nitrogen (O_2 and H_2O content less than 1 ppm). Solvents were purified by distillation under argon using appropriate drying agents.

2.2. Preparation of cation-exchanged smectites.

Exchanged smectites were prepared by a cation-exchange reaction using NH_4Cl, $AlCl_3$ or H_2SO_4 solutions, respectively. To obtain smectite/M^{n+} (M^{n+} = NH_4^+ or Al^{+3}); 10 g of the desired smectite was suspended in an aqueous solution of the chosen salt with a concentration of 10 times the CEC of the smectite. After stirring for 8 h at room temperature, the suspension was centrifuged at 10 °C with a velocity of 16000 rpm for 20 min. The supernatant liquid was removed and the procedure was repeated four times. The smectite/Al^{+3} was repeatedly washed and filtered until the filtrate was Cl^- free.

Samples were dried at room temperature for one week and finely hand ground in an agate mortar.

Acid treatment was achieved by preparing a suspension of 10 g of the desired smectite (smectite/H^+) in 50 ml of H_2SO_4 1.5 M, which was then heated at 80 °C over 4 h for MMt and 3 h for Hect. The resulting solid was washed, until it was free of sulphate ions, with hot distilled water, collected by centrifugation and then dried at room temperature for 1 week.

2.3. Support activator preparation.

A suspension of 5 g of the desired smectite in 150 ml of toluene was prepared in a 250 ml round-bottom flask fitted with a tap. A dropping funnel containing trimethylaluminium (TMA 2 M in toluene, Aldrich) in a proportion of 17.3 x 10^{-3} Al mol/ 1g of smectite was connected to the round-bottom flask, and the system was closed using a gas bubbler to follow gas evolution. TMA solution was added dropwise to the suspension and the resulting mixture was stirred for 3 h at room temperature. The solid sample was then filtered, and washed twice with 50 ml of toluene and once with 50 ml of hexane, for 30 min each time. The final solid was dried in the vacuum line for 1 h. It was stored in the globe box at –20 °C. We designate the support activator obtained as smectite (name of the clay mineral used)/M^{n+} (cation in the interlaminar space)/TMA.

2.4. Ethylene polymerization experiments.

In the globe box in a 100 ml Schlenk 1.5 g of support activator was suspended in 50 ml of toluene and then 7 x 10^{-5} mol of the precatalyst was added. The mixture was allowed to react for 1 h at room temperature to prepare the catalytic system. After this time the solvent was removed and the resulting mixture was washed twice with 50 ml of fresh toluene for 30 min each time and dried in the vacuum line. The catalytic system was charged in the reactor containing 1 ml of tri*iso*butylaluminium (TIBA 1 M, Aldrich) and 50 ml of toluene. . The reactor was thermostatized at 50 °C and ethylene was supplied and the pressure was maintained continuously at 1 atm during the polymerization reaction. At the end of the reaction period, the remaining ethylene was removed and the reaction was stopped by adding acidified ethanol. The powdered polyethylene was recovered by filtration. The catalytic activity was calculated from the weight of polyethylene and the amount of metallocene complex used.

2.5. Materials Characterization.

X-Ray Fluorecense measurements (XRF) were performed using a spectrophotometer AXIOS PW4400 (PANalytical) with a rhodium anode as radiation source, at the X-ray laboratory of CITIUS (University of Sevilla). Samples were diluted at 10% p/p in wax and supported in boric acid tablets.

Attenuated Total Reflectance Infrared spectra (IR-ATR) were recorded, at the ICMS (CSIC-University of Sevilla), using a spectrophotometer JASCO-FT/ IR-6200 with a mercury radiation source, equipped with a simple reflection horizontal accessory with diamond crystal JASCO ATR PRO470-H. The operating conditions were 2600 scans with 4 cm^{-1} resolution in ambient corrections. The wave number range was 600–4000

cm^{-1} studied consistent with the spectrometer beam splitter and the microscope detector (JASCO MCT-M).

X-Ray Diffraction (XRD) patterns were recorded using a diffractometer PANanalytical X'Pert PRO, at the ICMS (CSIC-University of Sevilla), with a Cu anode and X'elerator detector, using Cu Kα radiation at 40 kV and 40 mA. Diffractograms were obtained from 3 to 70° 2θ at a scanning speed of 0.05° 2θ/ min and with a counting time of 3 s.

The thermal analyses (Thermogravimetric Analysis- Differential Thermal Analysis, TGA-DTA and Differential Scanning Calorimetry, DSC) were conducted under environmental conditions using an STD Q600 analyser (TA Instruments), at the ICMS (CSIC-University of Sevilla), with a temperature range from 30 to 1000 °C and a heating rate of 10 °C/min. DSC tests were carried out under a nitrogen atmosphere performing 2 heating cycles in the temperature range of 50–200 °C with a heating rate of 10 °C/min. Between 30 and 50 mg of sample were used for each measurement.

Scanning Electron Microscopy (SEM) was carried out in a JEOL JSM 5400 microscope equipped with a LINK Pentafet probe and ATW windows for Energy Dispersive X-ray Analysis (EDX) at the ICMS (CSIC-University of Sevilla).

Magic Angle Spinning Nuclear Magnetic Resonance MAS-NMR experiments were performed on a Bruker DRX 400 spectrometer, at the ICMS (CSIC-University of Sevilla), equipped with a 4-mm multinuclear probe, operating at 400.13, 79.49 and 104.26 MHz for ^{1}H, ^{29}Si and ^{27}Al, respectively. Powdered samples were packed into zirconia rotors spinning at 10 kHz. Chemical shifts of nuclei (reported in ppm) were measured with respect to $SiMe_4$ for both proton and silicon, and to $[Al(H_2O)_6]^{3+}$ for aluminium. ^{1}H MAS-NMR spectra were obtained using typical $\pi/2$ pulse widths of 4.1 μs and a pulse spacing of 5 s. ^{29}Si MAS-NMR spectrum was obtained using a pulse

length of 2.7 μs (π/2 pulse length = 7.1 μs) with pulse spacing from 3 to 60 s. Finally, ^{27}Al MAS-NMR spectra were obtained using a pulse length of 0.92 μs (π/2 pulse length = 9.25 μs) with delay time from 3 to 60 s.

3. Results and discussion

3.1. X-Ray Fluorescence (XRF).

The XRF technique was used to confirm the chemical composition of the clays. The compositions of starting materials (see Supporting information) fit with the chemical analysis given by the provider. The results for the exchanged clays are consistent with the introduction of the corresponding cation in the interlayer space. Table 1 shows the XRF results of the samples after the TMA had reacted; the high content of Al_2O_3 compared with the starting materials confirmed that the reaction with TMA was successful.

Table 1.

Chemical composition of the support activators obtained from MMt determined by XRF.

Chemical Composition[(a)]	**MMt/TMA (% w/w)**	**MMt/Al/TMA (% w/w)**	**MMt/NH_4/TMA (% w/w)**	**MMt/H/TMA (% w/w)**
SiO_2	49.7	43.8	55.0	48.0
Al_2O_3	38.9	49.9	37.0	47.0
Fe_2O_3	2.1	1.8	1.8	1.2

MgO	5.5	3.9	5.4	3.1
Na_2O	1.2	0.1	-	-
CaO	1.0	-	-	0.2
K_2O	0.3	0.2	0.3	0.2
TiO_2	0.4	0.3	0.4	0.3
MnO	0.1	-	0.1	-
F, Cl	0.8	-	-	-

Table 2.

Chemical composition of the support activators obtained from Hect determined by XRF.

Chemical Composition	**Hect/TMA (% w/w)**	**Hect/Al/TMA (% w/w)**	**Hect/NH_4/TMA (% w/w)**	**Hect/H/TMA (% w/w)**
SiO_2	32.6	44.2	46.8	78.9
Al_2O_3	32.3	11.7	14.8	7.9
Fe_2O_3	0.2	0.2	0.5	01
MgO	11.1	16.2	16.2	0.1
Na_2O	0.2	0.1	0.1	-
CaO	0.6	0.1	0.1	0.0
K_2O	0.1	0.2	0.2	0.0
TiO_2	0.0	0.0	0.0	-
MnO	0.0	-	-	-
F, Cl	1.8	3.3	29	1.5

C.L[(a)]	21.1	23.8	18.4	11.5

[(a)] C.L: Calcination loss.

3.2. X-Ray Diffraction (XRD).

The XRD patterns of the starting materials, before and after homoionization with the different cations, showed a set of reflections consistent with the patterns found in the literature for each[25, 26]. The interplanar spacing (*d*-values) calculated from the reflections also corresponded well with literature data [25, 26]. These patterns (Table 3) reveal the highly crystalline nature of the samples. For the dioctahedral clay minerals (Fig. 2), the *001* reflection shifts from 5.83° 2θ (MMt, d_{001} = 15.16 Å) to 5.99° 2θ (MMt/TMA, d_{001} = 14.76 Å). For the trioctahedral clay minerals (Fig. 3), the *001* reflection shifts from 5.90° 2θ (Hect, d_{001} = 14.97 Å) to 5.80° 2θ (Hect/TMA, d001 = 15.23 Å). Only in the case of acid treatment XRD parameters indicate a partial destruction of the structure for MMt/H and a total destruction for Hect/H, where the signals corresponding to hectorite were absent.

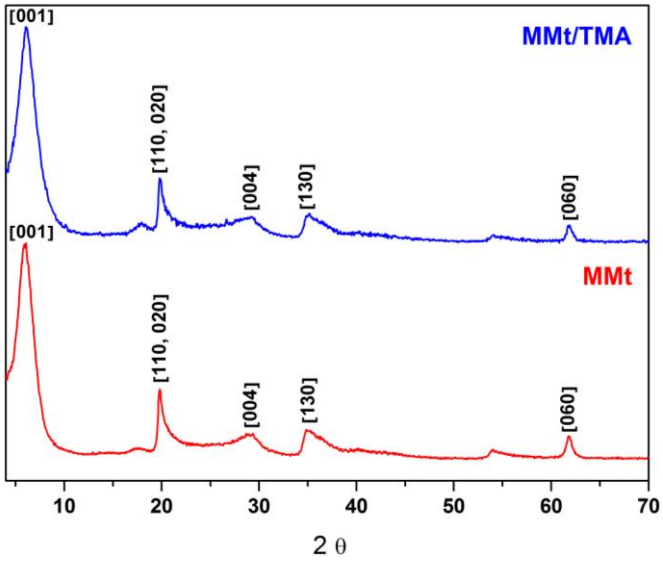

Fig. 2. Diffraction patterns and signal assignment for MMt and MMt/TMA.

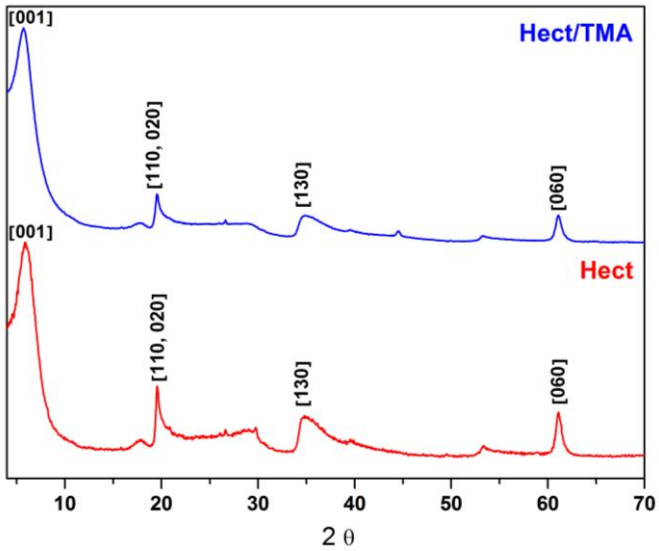

Fig. 3. Diffraction patterns and signal assignment for Hect and Hect/TMA.

In the TMA treated samples, the shift of the *001* reflection towards higher angles ,with a consequent diminution of the basal spacing, indicates [27] the reaction takes place not only with water molecules outside the layers of the clay but also with the water molecules located in the interlayer space. However, for Hect the tendency is the opposite, indicating a different reaction pattern of the TMA compound with this smectite.

Table 3.

Selected reflections of the materials.

Material	Reflection 001		Reflection 060	
	Pos. [°2θ]	**d_{001} [Å]**	**Pos. [°2θ]**	**d_{060} [Å]**
MMt	5.83	15.16	61.81	1.50
MMt/TMA	5.99	14.76	61.81	1.50
Hect	5.90	14.97	61.06	1.52
Hect/TMA	5.80	15.23	61.06	1.52
MMt/Al	5.64	15.68	61.90	1.50
MMt/Al/TMA	5.98	14.77	61.65	1.50
MMt/H	5.78	15.30	61.78	1.50
MMt/H/TMA	5.90	14.99	61.83	1.50
MMt/NH_4	7.25	12.19	61.85	1.50
MMt/NH_4/TMA	7.63	11.60	61.72	1.50
Hect/Al	5.94	14.87	61.13	1.52
Hect/Al/TMA	6.30	14.03	61.09	1.52
Hect/NH_4	7.14	12.39	61.08	1.52
Hect/NH_4/TMA	7.18	12.32	60.99	1.52

Material	Reflection	
	Pos. [°2θ]	**d_{001} [Å]**
Hect/H	21.72	4.093
Hect/H/TMA	22.18	4.009

3.3. Attenuated Total Reflectance Infrared Spectroscopy (*IR-ATR).*

The characteristic signals [28-30] assigned to the stretching vibrations of OH groups occur in the interval from 4000 to 3400 cm^{-1}. The bands corresponding to the Si-O-Si bonds of the tetrahedral layer of the smectites appear at around 1000 and 980 cm^{-1}. In MMt the expected isomorphic substitution of Al^{+3} by Mg^{+2} in the octahedral sheets of the layers is detected by the signals at 832 and 635 cm^{-1}, owing to Al-OH-Mg and Mg-OH-Mg bending vibrations, respectively [31, 32]. In Hect the band at 689 cm^{-1} is assigned to a Si-O-Al bending vibration, which suggests the presence of impurities in the sample that failed to be eliminated during purification. The unexpected signal at 793 cm^{-1} is consistent with the presence of quartz in the sample; both observations are explained by the natural origin of Hect.

The IR-ATR data are consistent with the preservation of the structure of the materials after interlayer cation exchange. The spectra for smectite/NH_4^+ showed the typical signal at 1440 cm^{-1} attributed to the bending vibration of the NH_4^+ cation [33]. The persistence of the signal at 980 cm^{-1} in MMt and 960 cm^{-1} in Hect was associated with Si-O-Si stretching bands, indicating that the layered structure of the original clay was not destroyed, except for Hect/H. As a result of the acid treatment the IR-ATR spectrum of Hect/H (Fig.4) reflects the structural degradation and the formation of an amorphous silica phase. The Si-O-Si stretching band in the original Hect is shifted to 1015 cm^{-1} due to the formation of this amorphous phase [34]. However, analysis of the bands of the MMt/H spectrum shows that structure is only slightly affected.

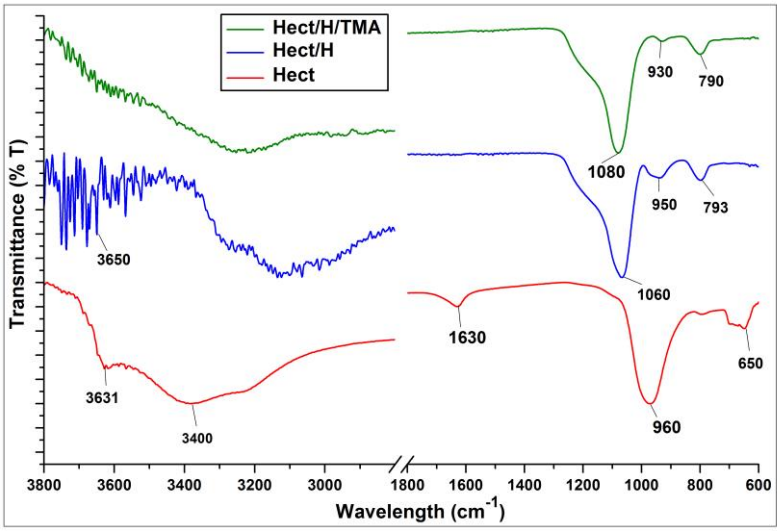

Fig. 4. IR-ATR spectra of Hect, Hect/H and Hect/H/TMA.

In the starting materials, the bands at 1623 cm^{-1}, H–O–H bending, and at 3400 cm^{-1}, stretching of water, are observed. These bands disappeared after TMA treatment and the new peaks observed at 2950 cm^{-1} typicals for Al-R bonds corroborated the incorporation of the aluminium compound into the smectite[35, 36]. For more information see the IR-ATR spectra of the samples in the supporting data.

3.3. Thermal analysis (TGA-DTA).

All TGA and DTA curves show three temperature regions indicating a weight loss at each step (see supporting information). The first weight loss region found around 30-225 °C is attributed to the loss of water, and the second observed in the interval 225-500 °C is explained by the dehydroxylation of the octahedral sheet [37]. The third region observed over 500 °C is explained by the decomposition of smectites. In the case of clays treated with TMA the first weight loss is lower than in the starting materials

because the molecules of water have previously reacted with the aluminium compound. However, in the third region the weight loss is greater, this result confirms that TMA has been incorporated in the solid matrix [38].

3.4. Magic Angle Spinning Nuclear Magnetic Resonance Spectroscopy (^{29}Si, ^{27}Al, ^{1}H MAS-NMR).

Solid-state MAS-NMR is known as a powerful technique to probe the structure, conformation, and dynamics of molecules at interfaces, so it was used to obtain more information of short-range structure.

Based on the structural characterization of smectites using ^{29}Si MAS-NMR, the resonance at –94 and –95 ppm for MMt (Fig.5) and Hect (Fig.6), respectively, is assigned to silicon atoms in the tetrahedral sheet with a Q^3(0Al) environment, typical of Si atoms present in smectites without isomorphic substitution in this sheet [39-41].

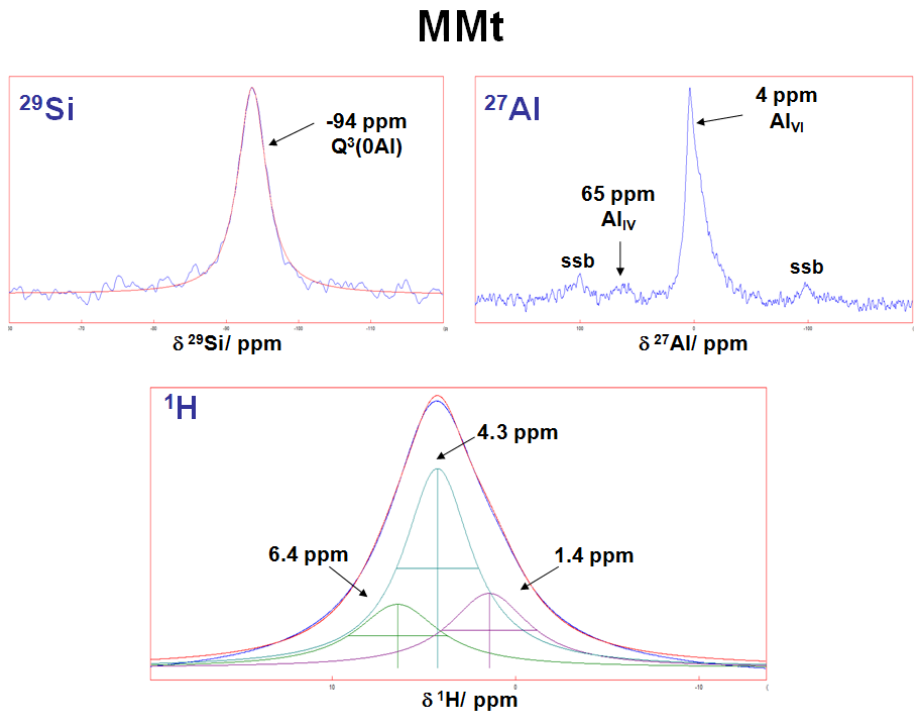

Fig. 5. ^{29}Si, ^{27}Al and ^{1}H MAS-NMR spectra of MMt.

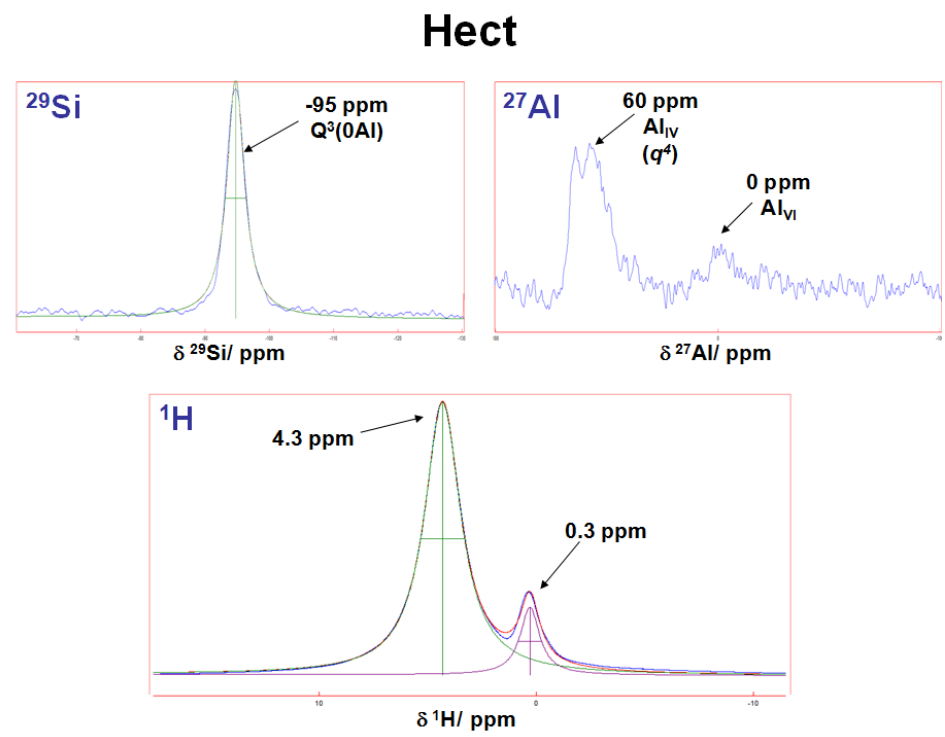

Fig. 6. ^{29}Si, ^{27}Al and ^{1}H MAS-NMR spectra of Hect.

MMt is a dioctahedral smectite containing aluminium and isomorphic magnesium substitutions in the octahedral sheet. Hect is a trioctahedral smectite containing magnesium in the octahedral sheet, and in this case the isomorphic substitutions are lithium atoms. Therefore, Hect has been selected because by definition, it has no structural aluminium. In phyllosilicates as MMt aluminium is in the octahedral sheet; and ^{27}Al MAS-NMR analysis reveals a peak at ca. 4 ppm which is related to this atom in the structural unit AlO_6 .The peak at ca. 65 ppm is assigned to aluminium in a tetrahedral environment resulting from isomorphic substitutions of silicon by aluminium in the tetrahedral sheet (structural unit AlO_4). Peaks observed for hectorite, which theoretically are not expected, denote the natural origin of this material. To analyse the way in which the aluminium compound interacts with the selected clays, ^{27}Al MAS-NMR spectroscopy was also performed. According to literature data [42-44] the reaction of TMA could take place with acidic protons of isolated silanol groups or with strained siloxane bridges. After TMA treatment three incompletely resolved signals are present at 60, 32, and 6 ppm, which are assigned to four-, five-, and six-coordinate aluminum species respectively (Fig. 7 for MMt/TMA and Fig. 8 for Hect/TMA) [45, 46]. The most remarkable observation in all samples is the detection of the new signal from pentahedral aluminium species (Al_v) only presented after TMA reaction. The working hypothesis is shown in figure 9 where this environment could be the result of a reaction with an acidic hydrogen that produced an Al-O-Si bond in which aluminium centre simultaneously interacts with a neighbouring silanol group [47, 48].

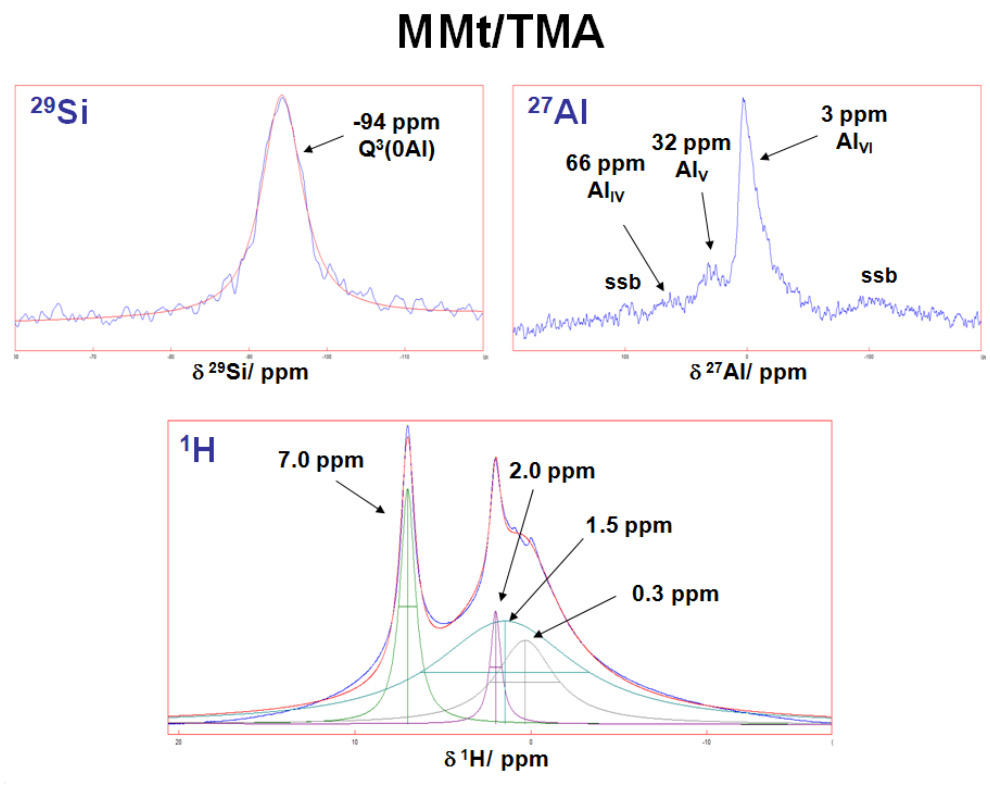

Fig. 7. ^{29}Si, ^{27}Al and ^{1}H MAS-NMR spectra of MMt/TMA.

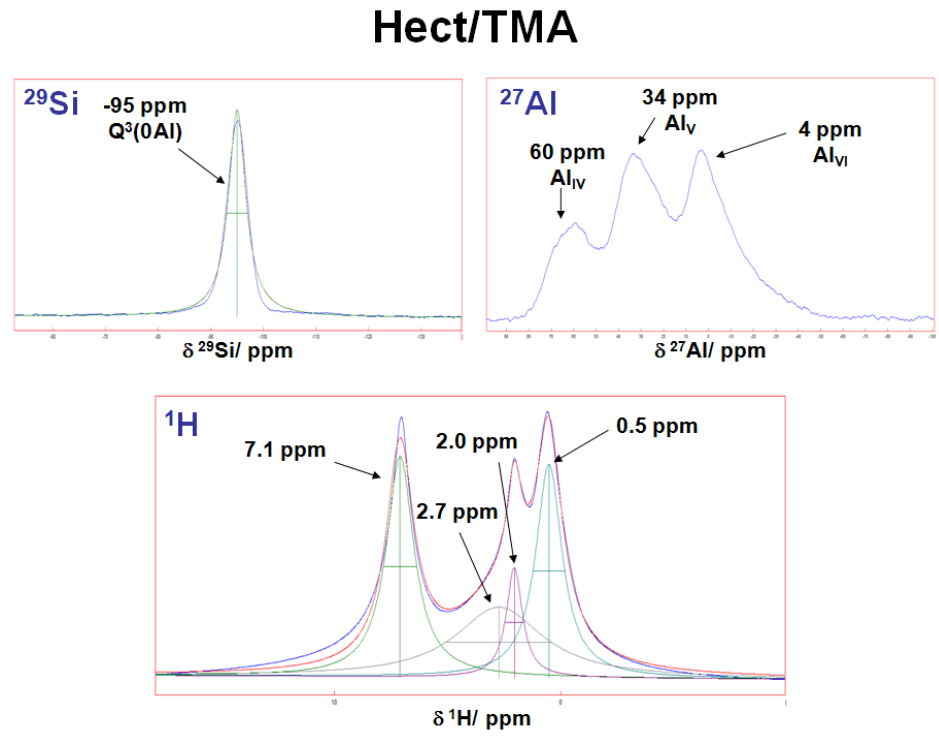

Fig. 8. ^{29}Si, ^{27}Al and ^{1}H MAS-NMR spectra of Hect/TMA.

For the starting material all signals of the ^{1}H NMR spectra have been conclusively assigned. For MMt the signal at 1.4 ppm corresponds to the structural hydroxyl groups of the material. In Hect ^{1}H NMR spectrum the same signal appears at 0.3 ppm. For both materials, the signal at 4.3 ppm is related to water in their structure. Finally, the signal at 6.4 ppm in MMt ^{1}H NMR spectrum corresponds to protons with Brönsted acidic character [49]. The treatment with TMA causes the appearance of new peaks corresponding to aliphatic protons in the range from 0 to –4 ppm, indicating a successful incorporation reaction of the aluminium compound [42]. The disappearance of the proton assigned to water molecules accords with the evidence obtained by other techniques. Moreover, since the polymerization activity of these materials can be poisoned by the presence of water, its elimination is crucial to ensure their use as cocatalysts. The most interesting feature is the presence of new signals corresponding to new acidic protons around 6.5–7.0 ppm which are only observed after TMA treatment, but not after interlaminar cation exchange. Althougt we can think toluene is responsible of this signal, we ruled out this fact because integrals are not in correspondence with the aliphatic signals and another techniques, as IR, do not show the signals for this solvent.

3.5. Study of ethylene polymerization behaviour.

[Zr(η^5-C_5H_5){η^5-$C_9H_6SiMe_2(CH_2CH=CH_2)$}$Cl_2$] previously synthesised by our research laboratory was selected as precatalyst due to its known activity in ethylene polymerization under homogeneous conditions (in the presence of MAO as cocatalyst (1:1000 Zr/Al) activity of 258.0 Kg PE/mol Zr.atm.h was obtained) together with the

potential role of the allyl moiety in the active species to provide stabilization [24]. It is noteworthy to emphasize that a non-methylated zirconocene compound has been employed, which consequently requires an initial *in situ* alkylation reaction to generate the active cationic species.

To obtain the heterogeneous system, the appropriate support activator was treated with a solution of the zirconocene compound and the supernatant solution was removed by filtration to ensure that no zirconium compound remained in the homogeneous phase. The activity values for the heterogeneous systems are in Table 4 with the best case (entry 7) showing around 27% activity, making it a very good option for potential industrial applications [50, 51].

Table 4.

Results of the characterization and performance of the support activators in ethylene polymerization.

Entry	Support Activator	g(Al_2O_3)TMA /100g support activator	Activity[(a)] (Kg PE/mol Zr.h.atm)
1	**Hect/TMA**	46.7	21
2	**MMt/Al/TMA**	54.7	29
3	**MMt/H/TMA**	56.2	9
4	**MMt/NH_4/TMA**	26.1	57
5	**Hect/Al/TMA**	7.3	23
6	**Hect/H/TMA**	8.4	3
7	**Hect/NH_4/TMA**	15.2	70

(a) Polymerization conditions; temperature = 50 °C, ethylene pressure = 1 atm., scavenger = TIBA (1mL), cat. $7x10^{-5}$ mol, solvent = toluene (50 mL).

3.6. Analysis of results and interpretation

Considering that the smectite layers act as non-coordinating anions (NCA), to stabilize the active species, the integrity in the structure seems to be crucial in explaining the catalytic activity. The CEC of the support activator has a direct role in determining [52] the number of active species that can be accommodated in the interlaminar space. At higher CEC more cationic species would be incorporated into the smectite, allowing more polymer production. Indeed, the most active material (entry 7, table 4) is derived from Hect (CEC = 245 meq/100g). Another point to consider is the structural stabilization of the cationic species responsible of the polymerization. The alteration of catalytic activities from the destruction of the structure of the support activator is evident after acid treatment (entry 3 and 6, table 4). Hect/H/TMA is practically inactive, in spite of its high CEC; this might be explained by the destruction of the layered stacking which prevents it acting as an NCA, demonstrated by the characterization techniques.

HDPE polyethylene samples were obtained from MMt/Al/TMA as evidenced by preliminary DSC characterization. During the ethylene polymerization, the MMT layers were exfoliated by the polymerization force exerted during propagation of the ethylene chain as inferred from the 001 reflection of the material analyzed by XRD after polymerization.

The XRF results demonstrated that there is not a direct correlation between the quantity of incorporated aluminium and polymerization activity. The smectite with most aluminium incorporated, whilst maintaining an unaltered structure, does not show

higher activity (entry 2, table 4). Nor does the most active MMt correspond with the level aluminium incorporated (entry 4, table 4). On the basis of these data we suggest that the catalytic activity depends mainly on the nature but not on the amount of the aluminium species on the support activator. Thus, we must consider that the most active material contains no structural aluminium (Hect). TMA treatment seems to be crucial to explain the catalytic activity found for these materials. In recent years some investigations [53-55] have postulated the formation of aluminoxanes through the reaction of the aluminium compound with residual water molecules in the clay. These aluminoxanes would act as activators in the reaction with the zirconium precatalyts. Our previous studies using TMA or TEA ruled out this hypothesis, rather they pointed to the acidity modification as responsible for the generation of the active species. So, the nature and strength of acid sites generated after the TMA reaction can be used to explain the mechanism to generate the active species in the polymerization reaction. In order to obtain a more detailed understanding of the nature of the active species, it seemed imperative to know the nature of the materials' acidity in terms of Brönsted and Lewis acid sites. The analysis of the MAS-NMR results gives rise to two observations: i) stronger Lewis acid sites were formed as a result of the TMA reaction (the pentahedral coordinated aluminium detected by ^{27}Al MAS-NMR analysis) and, ii) the formation of new Brönsted acid sites was observed by ^{1}H MAS-NMR only after TMA treatment. It is well known [56-60] that Lewis acids induce Brönsted acidity by coordinating protic species to a metal centre, thereby polarizing an E-H bond and rendering samples with enhanced Brönsted acidity. We interpret our experimental results as a consequence of a cooperative effect between the hydroxyl groups in the matrix and the new Lewis acid sites (Fig. 6), which are aluminium centres generated by

TMA. Thus, TMA treatment must render a metal Lewis acid centre that interacts with the OH bond to generate new Al_V-(OH)-Si groups. Consequently, the incorporation of TMA in the smectite would generate materials with more acidic properties than the parent materials, thus generating more of the active species responsible of the polymerization. The acidity was modulated by altering the interlaminar cation with Hect/NH_4/TMA and MMt/NH_4/TMA proving to be the most active support activators. Overall, these facts point towards the importance of the resulting acidity in ethylene polymerization for either the mechanism of formation or the stabilization (or both) of these support-activator.

Studies varying the Al(TMA)/smectite ratio, employing alternative precatalysts and olefins are continuing .

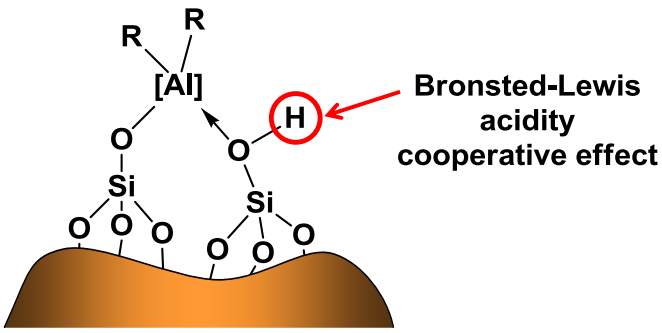

Fig. 9. Cooperative effect between Brönsted and Lewis acidic sites.

4. Conclusions

A series of MMt/M^{n+}/TMA and Hect/M^{n+}/TMA have been used as support activators with a zirconocene compound for ethylene polymerizations with good results in the absence of MAO. From the present results we concluded the performance of these materials as cocatalyst does not depend on the number aluminium species incorporated,

rather on the nature of these species on the clay. Careful characterisation of the support activators shows that the pentahedral aluminium is responsible for cationic species formation. These aluminium species result from a synergistic effect between the aluminium centres produced after TMA reaction and the SiOH groups located in the clay which generate more acidic protons than the starting materials. This cooperative effect may be responsible for active species generation. The present work again corroborates the important role that acidity may play in the generation of active species as well as the structural features contributing to the stabilization of the cationic species active in polymerization.

Acknowledgments. We would like to thank the DGICYT and FEDER funds (project CTQ 2010-14874) for their financial support. **and to the** Dirección General de Investigación Científica y Técnica (Projects MAT2007-60997 and CTQ2007-63297), Comunidad Autónoma de Madrid: (Project S-0505-PPQ/0328-02).

Appendix A. Supporting information associated with this article can be found, in the online version.

References

[1] H. Sinn, W. Kaminsky, H.J. Vollmer, R. Woldt, Angewandte Chemie-International Edition in English 19 (1980) 390-392.

[2] H.G. Alt, A. Koppl, Chemical Reviews 100 (2000) 1205-1221.

[3] G.W. Coates, Chemical Reviews 100 (2000) 1223-1252.

[4] W. Kaminsky, Catalysis Today 62 (2000) 23-34.

[5] D.E. Babushkin, N.V. Semikolenova, V.A. Zakharov, E.P. Talsi, Macromolecular Chemistry and Physics 201 (2000) 558-567.

[6] V.A. Zakharov, E.P. Talzi, Zakharov, II, D.E. Babushkin, N.V. Semikolenova, Kinetics and Catalysis 40 (1999) 836-850.

[7] E.P. Talsi, N.V. Semikolenova, V.N. Panchenko, A.P. Sobolev, D.E. Babushkin, A.A. Shubin, V.A. Zakharov, Journal of Molecular Catalysis a-Chemical 139 (1999) 131-137.

[8] D.E. Babushkin, N.V. Semikolenova, V.N. Panchenko, A.P. Sobolev, V.A. Zakharov, E.P. Talsi, Macromolecular Chemistry and Physics 198 (1997) 3845-3854.

[9] R. Huang, R. Duchateau, C.E. Koning, J.C. Chadwick, Macromolecules 41 (2008) 579-590.

[10] K. Ikenaga, S. Chen, M.-a. Ohshima, H. Kurokawa, H. Miura, Catalysis Communications 8 (2007) 36-38.

[11] J.R. Severn, J.C. Chadwick, R. Duchateau, N. Friederichs, Chemical Reviews 105 (2005) 4073-4147.

[12] V. Tabernero, C. Camejo, P. Terreros, M. Dolores Alba, T. Cuenca, Materials 3 (2010) 1015-1030.

[13] M.F. Brigatti, E. Galan, B.K.G. Theng, in: F. Bergaya, G. Lagaly, B.K.G. Theng (Eds.), Handbook of Clay Science. Developments in Clay Science, Elsevier, 2011, pp. 19-86.

[14] G. Centi, S. Perathoner, Microporous and Mesoporous Materials 107 (2008) 3-15.

[15] A. Vaccari, Applied Clay Science 14 (1999) 161-198.

[16] U. Flessner, D.J. Jones, J. Roziere, J. Zajac, L. Storaro, M. Lenarda, M. Pavan, A. Jimenez-Lopez, E. Rodriguez-Castellon, M. Trombetta, G. Busca, Journal of Molecular Catalysis a-Chemical 168 (2001) 247-256.

[17] G. Busca, Physical Chemistry Chemical Physics 1 (1999) 723-736.

[18] E. Finocchio, G. Busca, S. Rossini, U. Cornaro, V. Piccoli, R. Miglio, Catalysis Today 33 (1997) 335-352.

[19] E.Y.X. Chen, T.J. Marks, Chemical Reviews 100 (2000) 1391-1434.

[20] L.J. Arroyo, H. Li, B.J. Teppen, S.A. Boyd, Clays and Clay Minerals 53 (2005) 511-519.

[21] A. Siregar, M. Kleber, R. Mikutta, R. Jahn, European Journal of Soil Science 56 (2005) 481-490.

[22] R. Mikutta, M. Kleber, K. Kaiser, R. Jahn, Soil Science Society of America Journal 69 (2005) 120-135.

[23] A. Czimerova, J. Bujdak, R. Dohrmann, Applied Clay Science 34 (2006) 2-13.

[24] J. Cano, P. Gomez-Sal, G. Heinz, G. Martinez, P. Royo, Inorganica Chimica Acta 345 (2003) 15-26.

[25] M. Mantovani, A. Escudero, M.D. Alba, A.I. Becerro, Applied Geochemistry 24 (2009) 1251-1260.

[26] S.J. Chipera, D.L. Bish, Clays and Clay Minerals 49 (2001) 398-409.

[27] P. Pushpaletha, S. Rugmini, M. Lalithambika, Applied Clay Science 30 (2005) 141-153.

[28] J.T. Kloprogge, S. Komarneni, K. Yanagisawa, R.L. Frost, R. Fry, Journal of Materials Science Letters 17 (1998) 1853-1855.

[29] J. Madejova, H. Palkova, M. Pentrak, P. Komadel, Clays and Clay Minerals 57 (2009) 392-403.

[30] J. Madejova, M. Pentrak, H. Palkova, P. Komadel, Vibrational Spectroscopy 49 (2009) 211-218.

[31] J. Bishop, J. Madejova, P. Komadel, H. Froschl, Clay Minerals 37 (2002) 607-616.

[32] J. Madejova, J. Bujdak, M. Janek, P. Komadel, Spectrochimica Acta Part a-Molecular and Biomolecular Spectroscopy 54 (1998) 1397-1406.

[33] S. Petit, D. Righi, J. Madejova, A. Decarreau, Clay Minerals 34 (1999) 543-549.

[34] P. Komadel, J. Madejova, M. Janek, W.P. Gates, R.J. Kirkpatrick, J.W. Stucki, Clays and Clay Minerals 44 (1996) 228-236.

[35] V.N. Panchenko, N.V. Semikolenova, I.G. Danilova, E.A. Paukshtis, V.A. Zakharov, Kinetics and Catalysis 40 (1999) 556-561.

[36] V.N. Panchenko, N.V. Semikolenova, I.G. Danilova, E.A. Paukshtis, V.A. Zakharov, Journal of Molecular Catalysis a-Chemical 142 (1999) 27-37.

[37] C.G.D. Skoubris E., Christidis G. E, Gionis V., Clays and Clay Mineral 61 (2013) 83-97.

[38] V.N. Panchenko, V.A. Zakharov, I.G. Danilova, E.A. Paukshtis, Zakharov, II, V.G. Goncharov, A.P. Suknev, Journal of Molecular Catalysis a-Chemical 174 (2001) 107-117.

[39] S.P. Altaner, C.A. Weiss, R.J. Kirkpatrick, Nature 331 (1988) 699-702.

[40] C.A. Weiss, S.P. Altaner, R.J. Kirkpatrick, American Mineralogist 72 (1987) 935-942.

[41] J. Sanz, J.M. Serratosa, W.E.E. Stone, Journal of Molecular Structure 141 (1986) 269-277.

[42] J. Li, J.A. DiVerdi, G.E. Maciel, Journal of the American Chemical Society 128 (2006) 17093-17101.

[43] R.L. Puurunen, A. Root, S. Haukka, E.I. Iiskola, M. Lindblad, A.O.I. Krause, Journal of Physical Chemistry B 104 (2000) 6599-6609.

[44] X. Cheng, Y. Liu, D. Chen, Journal of Physical Chemistry A 115 (2011) 4719-4728.

[45] S. Milione, G. Milano, L. Cavallo, Organometallics 31 (2012) 8498-8504.

[46] D. Lee, H. Takahashi, A.S.L. Thankamony, J.-P. Dacquin, M. Bardet, O. Lafon, G. De Paepe, Journal of the American Chemical Society 134 (2012) 18491-18494.

[47] A.A. Gurinov, Y.A. Rozhkova, A. Zukal, J. Cejka, I.G. Shenderovich, Langmuir 27 (2011
) 12115-12123.

[48] E.J.M. Hensen, D.G. Poduval, P.C.M.M. Magusin, A.E. Coumans, J.A.R. van Veen, Journal of Catalysis 269 (2010) 201-218.

[49] M.D. Alba, A.I. Becerro, M.A. Castro, A.C. Perdigon, J.M. Trillo, Journal of Physical Chemistry B 107 (2003) 3996-4001.

[50] T. Vestberg, P. Denifl, C.-E. Wilén, J. Appl. Polym. Sci. 110 (2008) 2021-2029.

[51] A.J.D. de Freitas, J.H.Z. dos Santos, S.M.P. Meneghetti, M.R. Meneghetti, J. Appl. Polym. Sci. 119 (2011) 3051-3057.

[52] D.A. Laird, Applied Clay Science 34 (2006) 74-87.

[53] H.-G.Z. Cai, Chun-Yu; Chen, Bin; Zhang, Xue-Quan; Zhang, He-Xin, Journal of Nanoscience and Nanotechnology 12 (2012) 7296.

[54] H. Kurokawa, S. Morita, M. Matsuda, H. Suzuki, M.-a. Ohshima, H. Miura, Applied Catalysis a-General 360 (2009) 192-198.

[55] C.B. Liu, T. Tang, B.T. Huang, Journal of Catalysis 221 (2004) 162-169.

[56] C. Chizallet, P. Raybaud, Angewandte Chemie-International Edition 48 (2009) 2891-2893.

[57] C. Chizallet, P. Raybaud, Chemphyschem 11 (2010) 105-108.

[58] F. Leydier, C. Chizallet, A. Chaumonnot, M. Digne, E. Soyer, A.-A. Quoineaud, D. Costa, P. Raybaud, Journal of Catalysis 284 (2011) 215-229.

[59] F. Leydier, C. Chizallet, D. Costa, P. Raybaud, Chemical Communications 48 (2012) 4076-4078.

[60] K. Wilson, J.H. Clark, Pure and Applied Chemistry 72 (2000) 1313-1319.

LIST OF TABLES, SCHEMES AND FIGURES IN THE ORDER OF APPEARANCE.

SUPPORTING INFORMATION

Fig. S17. ^{29}Si, ^{27}Al and ^{1}H MAS-NMR spectra of Hect/H/TMA.

Fig. S18. ^{29}Si, ^{27}Al and ^{1}H MAS-NMR spectra of Hect/NH_4.

Fig. S19. ^{29}Si, ^{27}Al and ^{1}H MAS-NMR spectra of Hect/NH_4/TMA.